Acta Metallurgica Sinica (English Letters) (2020) 33:913–921
https://doi.org/10.1007/s40195-020-01038-8

Enhancing High-Temperature Strength and Thermal Stability of Al_2O_3/Al Composites by High-Temperature Pre-treatment of Ultrafine Al Powders

Yu-Ning Zan[1,3] · Yang-Tao Zhou[1] · Xiao-Nan Li[1,3] · Guo-Nan Ma[1,3] · Zhen-Yu Liu[1] · Quan-Zhao Wang[2] · Dong Wang[1] · Bo-Lv Xiao[1] · Zong-Yi Ma[1]

Received: 16 January 2020 / Revised: 12 February 2020 / Published online: 15 April 2020

Abstract

Amorphous Al_2O_3-reinforced Al composite (am-Al_2O_3/Al) compacted from ultrafine Al powders for high-temperature usages confronts with drawbacks because crystallization of am-Al_2O_3 at high temperatures will result in serious strength loss. Aiming at this unsolved problem, in this study, high-temperature Al materials with enhanced thermal stability were developed through introducing more thermally stable nano-sized particles via high-temperature pre-treatment of ultrafine Al powders. It was found that the pre-treatment at ≤ 550 °C could introduce a few Al_2O_3 in the Al matrix and increase the strength of the composites, but the strength was still below that of am-Al_2O_3/Al because without being pinned firmly, grain boundaries (GBs) were softened at high temperature and intergranular fracture happened. When the pre-treatment was carried out at 600 °C, nitridation and oxidation processes happened simultaneously, producing large numbers of intergranular (AlN + γ-Al_2O_3) particles. GB sliding and intergranular fracture were suppressed; therefore, higher strength than that of am-Al_2O_3/Al was realized. Furthermore, the (AlN + γ-Al_2O_3)/Al exhibited more superior thermal stability compared to am-Al_2O_3/Al for annealing treatment at 580 °C for 8 h. Therefore, an effective way to fabricate high-temperature Al composite with enhanced thermal stability was developed in this study.

Keywords Aluminum matrix composites · Particles · High-temperature strength · Thermal stability

1 Introduction

Al alloys are widely used for room temperature usages due to their superior formability, high strength and low density [1–3]. Nevertheless, Al materials with long-term stable strength at over 300 °C are further desired in some special applications such as pistons, fuselage bulkheads, wing skins, heat-resistant conductors and neutron absorber materials [4–7]. However, age-hardened Al alloys exhibiting prominent properties at room temperature (RT) usually lose their strength at high temperature, because precipitates such as Mg_2Si, $CuAl_2$, $MgZn_2$ would coarsen/dissolve and lose strengthening efficacy rapidly at ~200 °C because of diffusion of alloying elements [4, 5, 8, 9].

Al matrix composites (AMCs) reinforced by nano-sized ceramic particles are expected to exhibit enhanced mechanical properties at elevated temperatures [1, 2, 10–12]. Thermally stable nano-sized ceramic particles distributed within the Al grains can pin the dislocations against gliding and climbing, and in the meantime, particles distributed at the

Available online at http://link.springer.com/journal/40195.

✉ Quan-Zhao Wang
qzhwang@imr.ac.cn

✉ Zong-Yi Ma
zyma@imr.ac.cn

[1] Shenyang National Laboratory for Materials Science, Institute of Metal Research, Chinese Academy of Sciences, 72 Wenhua Road, Shenyang 110016, China

[2] Key Laboratory of Nuclear Materials and Safety Assessment, Institute of Metal Research, Chinese Academy of Sciences, 72 Wenhua Road, Shenyang 110016, China

[3] School of Materials Science and Engineering, University of Science and Technology of China, 72 Wenhua Road, Shenyang 110016, China

grain boundaries (GBs) can hinder GB sliding/migration and grain rotation, resulting in enhanced high-temperature strength [7, 13, 14].

It was recently reported that intergranular particles exhibited higher strengthening efficiency than intragraunular ones in Al_2O_3-reinforced Al composites (Al_2O_3/Al) [15]. Since the quantity of nano-sized particles which can be uniformly distributed in Al matrix is highly limited, the realization of higher strength depends more on the strengthening efficiency. Therefore, optimizing the spatial distribution of reinforcements is crucial for developing high-temperature Al materials [16].

Extraordinary strengthening efficiency was realized in Al_2O_3/Al fabricated by sintering ultrafine Al powders [9, 17]. It could be attributed to that lamellar amorphous Al_2O_3 (am-Al_2O_3) film on the surface of Al powders was distributed exactly at the GBs of the Al matrix. Balog et al. [17] reported that the tensile strength of 1.2 vol% Al_2O_3/Al at 300 °C reached 105 MPa. The positive strengthening efficiency indicated a promising prospect of pursuing high strength at high temperature.

However, Al_2O_3/Al mentioned above suffered a significant drawback.When the composites experienced a temperature higher than a critical value (about 450 °C) in the fabrication process, lamellar am-Al_2O_3 would transform into particulate γ-Al_2O_3 [18–20]. This could disrupt the interconnectivity of Al_2O_3 at the GBs and result in serious damage to the mechanical properties of the composites [18]. Clearly, this situation brings difficulties to conventional hot-pressing and deforming processes. More seriously, once the temperature in any preparation/service process exceeds the critical value for a certain period, permanent strength damage would be caused. Therefore, the application of this kind of Al_2O_3/Al is restricted by the deficient thermal stability of am-Al_2O_3.

Since γ-Al_2O_3 is much more stable at high temperatures, γ-Al_2O_3/Al with enhanced high-temperature strength can be developed if the quantity of γ-Al_2O_3 can be increased to remedy its lower strengthening efficiency. One feasible and inexpensive idea is pre-treating the ultrafine Al powders in air at high temperature to introduce more Al_2O_3. However, a major difficulty is that the am-Al_2O_3 film will inhibit the oxidation process. Therefore, the high-temperature treatment may exert obvious effects only after am-Al_2O_3 transforms into γ-Al_2O_3 and the underlying Al matrix is exposed.

It was reported that at about 590 °C in N_2 atmosphere, N_2 could react with Al powders to produce AlN nanoparticles, which could be utilized to enhance the high-temperature strength [16, 21, 22]. Therefore, the feasibility of introducing nanoparticles into the Al matrix in air atmosphere with appropriate treatment temperature is worth investigating. However, such study has not been reported to the best of our knowledge.

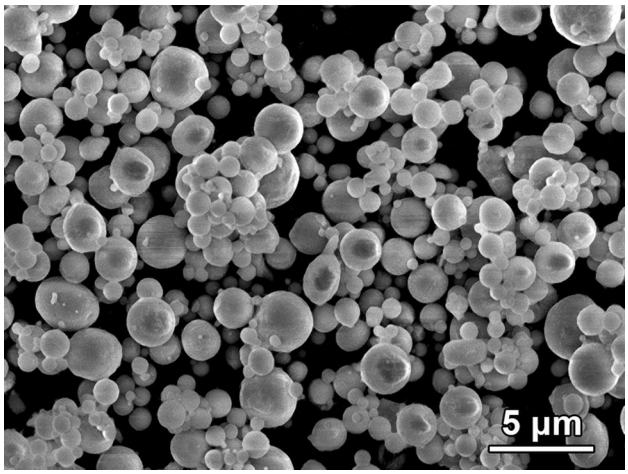

Fig. 1 SEM image of ultrafine Al powders used in this study

Table 1 Fabrication processes of the composites

Sample	Pre-treatment temperature (°C)	Hot-pressing temperature (°C)	Hot-pressing pressure (MPa)
400	400	630	50
500	500	630	50
550	550	630	50
600	600	630	50
AM	None	450	200

In the present study, ultrafine Al powders were utilized to fabricate the composites for high-temperature application. The aims of this study are (a) to elucidate the feasibility of introducing more nano-sized particles by high-temperature pre-treatment, (b) to study the influence of treatment temperature on the microstructure and mechanical properties of the composites, and (c) to develop a new kind of Al matrix composites with enhanced high-temperature strength and thermal stability.

2 Experimental

Ultrafine Al powders with an average diameter of 1.45 μm were used as raw material (Fig. 1). Different fabrication procedures of the samples are listed in Table 1. For samples 400, 500 and 550, ultrafine Al powders were heated in the furnace with air atmosphere for 2 h at 400 °C, 500 °C and 550 °C, respectively, and then cooled down in the furnace to RT. For sample 600, direct high-temperature treatment at 600 °C could lead to sintering or inflammation. Therefore, the Al powders were first cold-pressed until a relative density of ~60% was obtained to decrease the exposed area. Then, high-temperature treatment was carried out.

Powder metallurgy technique was applied to fabricate bulk materials. Hot pressing was carried out in a vacuum chamber of 10^{-2} Pa. Temperature was raised to 630 °C and kept for 2 h, and then, a pressure of 50 MPa was used to realize densification. According to Ref. [17], low hot-pressing temperature could maintain the amorphous state of Al_2O_3. Therefore, although hot-pressing temperature of 450 °C is usually not enough for densifying the composites under usual fabrication parameters, a composite was still fabricated at 450 °C, but a much higher pressure of 200 MPa was used to realize densifying (Sample AM) for the purpose of comparison. Finally, the billets were all extruded at 450 °C with an extrusion ratio of 18:1.

Microstructure and fractographs were examined using field emission scanning electron microscopy (FESEM, Leo Supra 55), and transmission electron microscopy (TEM, FEI Tecnai F20). Thin foil specimens for TEM observation were prepared by mechanical polishing and dimpling, followed by ion-milling using Gatan PIPS 695. X-ray diffractometer (XRD, D-MAX/2400 using Cu *K*α radiation) was used to analyze the composition of the composites.

Tensile specimens 5 mm in gauge length, 1.6 mm in width and 1.2 mm in thickness were machined parallel to the extrusion direction. Tensile test was carried out at both RT and 350 °C using Instron 5582 tester. A strain rate of 1×10^{-3} s^{-1} was used. To test the thermal stability, some of the samples were annealed at various temperatures for up to 8 h and then tested at 350 °C. To confirm the reason for strength loss of annealed sample AM, TEM examination was carried to observe the microstructure of sample annealed at 580 °C for 2 h.

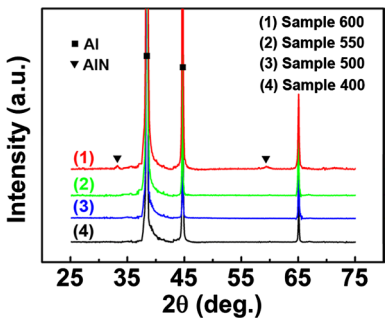

Fig. 2 XRD patterns of the composites

3 Results

3.1 Microstructure of the Composites

XRD patterns of samples pre-treated at different temperatures are shown in Fig. 2. Since the hot-pressing temperature of 630 °C was higher than the crystallization temperature of am-Al_2O_3, it can be expected that γ-Al_2O_3 was formed in these composites. However, the peaks of γ-Al_2O_3were not observed in all the samples, which might be attributed to its small quantity. For sample 600, the peaks of AlN were detected.

Figure 3 shows the microstructure of sample 500. In Fig. 3a, an ultrafine grain structure was revealed. A mass of nano-sized particles were observed (Fig. 3b), which were confirmed as γ-Al_2O_3 in our previous studies [15, 23]. It can be understood that am-Al_2O_3 at the GBs transformed into γ-Al_2O_3 in the hot-pressing process. During the extrusion process, grain rotation and grain boundary migration further happened, resulting in grain coalescence [13, 24, 25]. So, γ-Al_2O_3 can be observed at the GBs as well as inside the grains (Fig. 3b).

Figure 4a–d shows the microstructure of sample 600 under different magnifications. In Fig. 4a, it could be seen that the grains were finer than those in sample 500. A mass of nano-sized particles (white arrows) exhibited a nearly continuous distribution mainly at the GBs (Fig. 4b, c). It is considered that a larger quantity of nano-sized particles could pin the GBs through Zener pinning [13]; therefore, GB sliding/migration and grain rotation were retarded, which

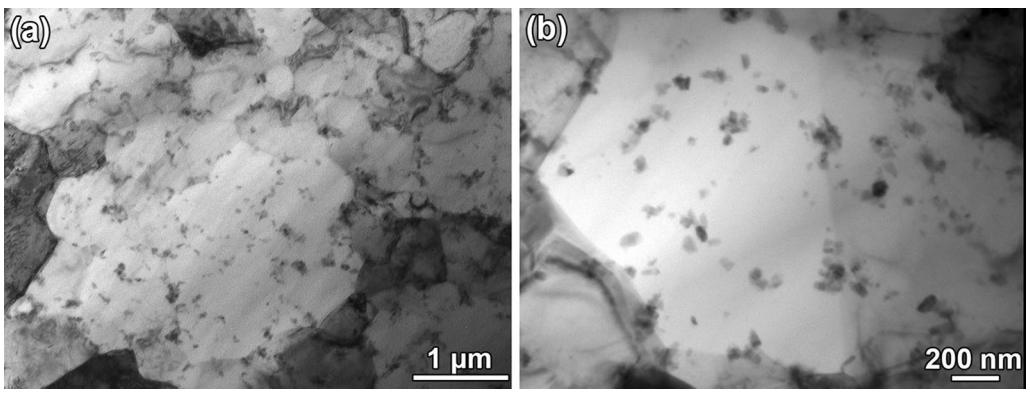

Fig. 3 TEM images showing microstructure (**a**) and GB-distributed γ-Al_2O_3 (**b**) in sample 500

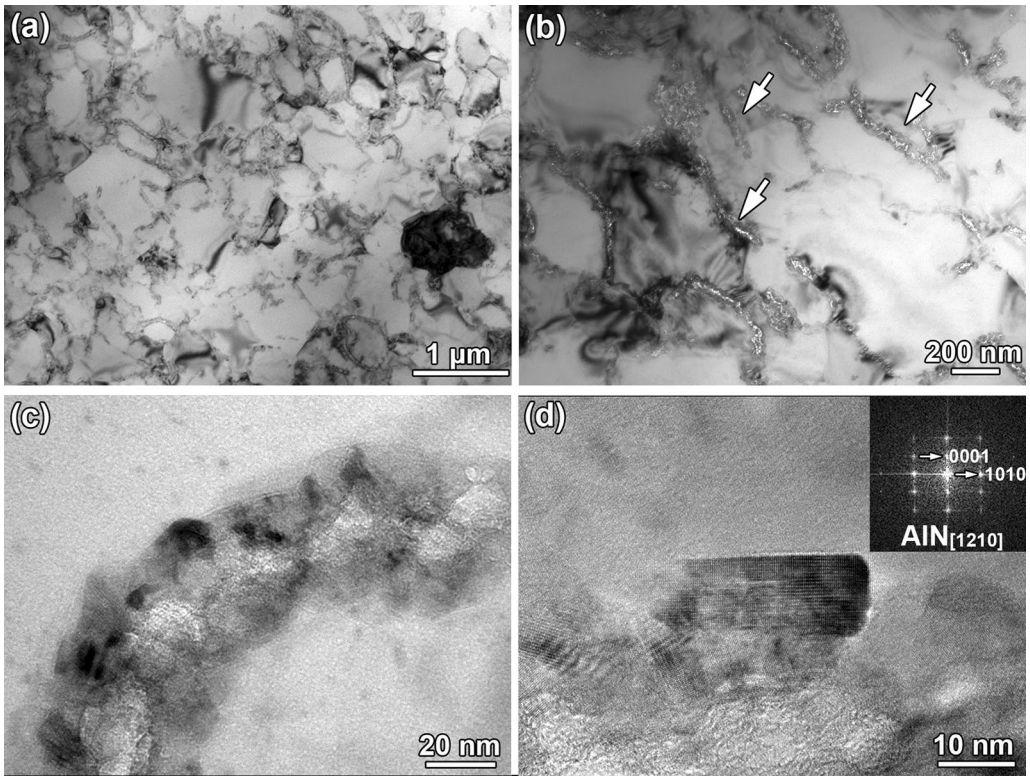

Fig. 4 TEM images showing grain structure **a**, GB-distributed nano-sized particles **b**, **c**, and HRTEM **d** of AlN particles in sample 600

could be confirmed by the GB distribution of the particles. In Fig. 4d, a high-resolution TEM (HRTEM) image revealed that some of the particles could be identified as AlN with a hexagonal structure. It indicated that the Al matrix reacted with N_2 in the air to produce AlN, which is consistent with the XRD result.

Figure 5 shows TEM image of sample AM. The grain structure of sample AM was similar to that of sample 600; however, the GB distributed Al_2O_3 was much thinner, as shown in Fig. 5b. Under the hot-pressing temperature of 450 °C, am-Al_2O_3 could remain its amorphous structure, as reported in Refs. [9, 18]. Despite its small quantity, am-Al_2O_3 with large surface area could cover the Al GBs adequately and prevent grains from coarsening, resulting in a finer structure than that in sample 500.

3.2 Mechanical Properties

Figure 6 shows the engineering stress–strain curves of the composites, and the tensile properties are listed in Table 2. It was revealed that with increasing pre-treatment temperature from 400 to 550 °C, the strength of the composites

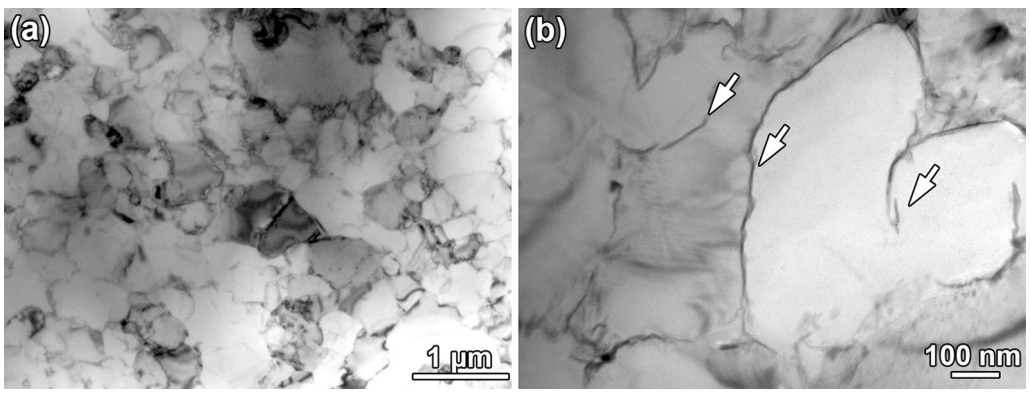

Fig. 5 TEM images showing microstructure **a** and GB-distributed am-Al_2O_3 (white arrows) **b** in sample AM

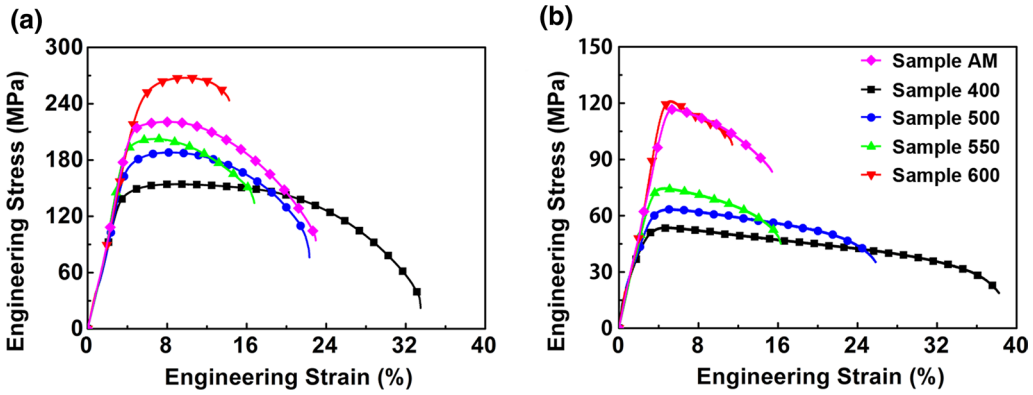

Fig. 6 Tensile engineering stress–strain curves for various composites at RT **a** and 350 °C **b**

Table 2 Tensile properties of the composites at RT and 350 °C

Sample	RT			350 °C		
	YS (MPa)	UTS (MPa)	El (%)	YS (MPa)	UTS (MPa)	El (%)
400	138 ± 3	154 ± 3	33 ± 6	39 ± 2	54 ± 1	37 ± 4
500	166 ± 4	188 ± 2	21 ± 3	48 ± 1	64 ± 2	25 ± 3
550	186 ± 4	203 ± 3	14 ± 4	61 ± 1	75 ± 2	15 ± 3
600	224 ± 3	268 ± 4	10 ± 4	113 ± 6	121 ± 1	6 ± 1
AM	197 ± 2	221 ± 2	21 ± 5	105 ± 4	117 ± 3	13 ± 2

YS Yield strength, *UTS* ultimate tensile strength and *El* elongation

increased gradually at both RT and 350 °C. However, the strength results indicated that a pre-treatment at temperatures ≤ 550 °C could not realize a composite strength comparable to that of sample AM. It is worth noting that when the treatment temperature increased to 600 °C, the strength of the composite exhibited a sharp rise and was higher than that of sample AM at both RT and 350 °C. It was also seen that with the increase in pre-treatment temperature, the ductility of the composites decreased.

3.3 Fractographs

Figure 7 shows the RT fracture surfaces of samples 400, 500 and 600. These fractographs exhibited a characteristic of obvious dimples. Furthermore, the dimple size decreased with increasing treatment temperature. The decrease in the dimple size implied the decrease in deformability. It was also disclosed that the fracture surfaces were smooth and only a few of particles were observed.

Figure 8 shows the fracture surfaces of samples 400, 500 and 600 at 350 °C. Unlike fracture surfaces at RT, an intergranular fracture characteristic is observed in Fig. 8a and c and also, the granules in Fig. 8c were finer than that in Fig. 8a. Particularly, in Fig. 8b and d, evident gaps (black arrows) indicated that relative gliding happened between the contiguous grains. A mass of nano-sized particles could be observed on the fracture surfaces (white arrows), indicating that the initiation location of fracture corresponded to the location of γ-Al_2O_3. It was also revealed that compared to Fig. 8b, more particles existed in Fig. 8d, indicating that more γ-Al_2O_3 was introduced at higher temperature.

In Fig. 8e, obviously different fractograph was observed in sample 600, in which some amount of dimple fracture characteristics were disclosed. It indicated that intergranular sliding and fracture were effectively suppressed. Some humps (white arrows) were observed on the fracture surfaces; however, the quantity of humps was smaller than that of the particles shown in Fig. 8b and d, indicating that most of the particles were not exposed on the fracture surface. They were also larger than the particles themselves as shown in Fig. 4, and this might be because of the Al matrix adhering to the particles. It can be speculated from these characteristics that fracture happened at the regions near the GBs instead of at the GBs in sample 600 at 350 °C.

3.4 Thermal Stability

Figure 9 highlights the enhancement in thermal stability of sample 600 compared to sample AM, by exhibiting tensile strength (at 350 °C) of samples AM and 600 after being annealed for up to 8 h. In a high-temperature environment of 550 °C and 580 °C, sample AM began to lose

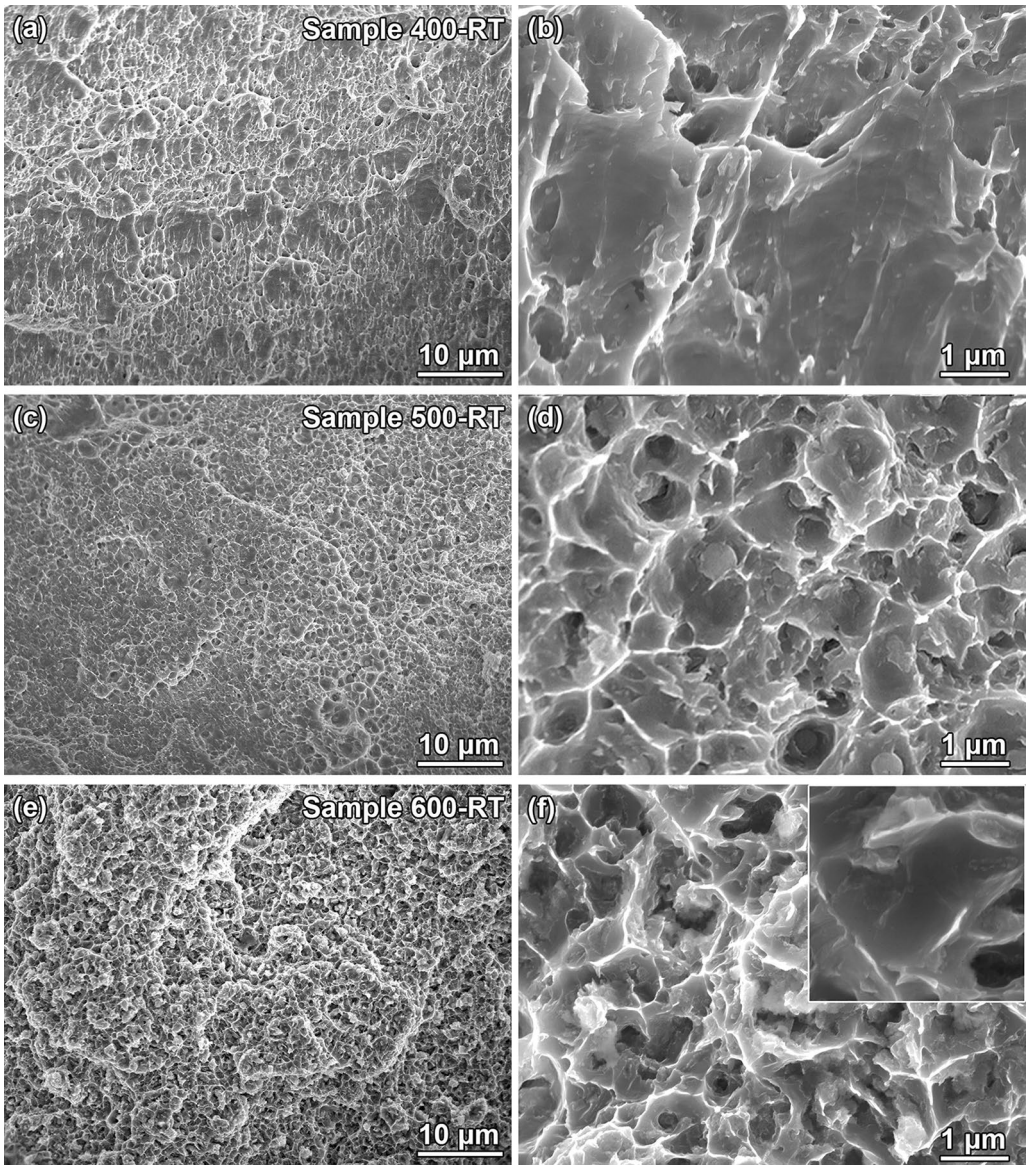

Fig. 7 SEM fractographs of samples 400 **a**, **b**, 500 **c**, **d** and 600 **e**, **f** at RT with different magnifications

its strength once the annealing process was carried out. Even at 520 °C, evident strength loss began to emerge after being annealed for 4 h. The marked difference, however, was that sample 600 exhibited a steady strength after an annealing process at 580 °C for 8 h, showing its significant advantage in thermal stability over alloys or composites in Refs. [4, 9, 17, 18].

The microstructure of sample AM annealed at 580 °C for 2 h is shown in Fig. 10, from which the reason for its strength loss can be analyzed. Although the Al grains were not coarsened (Fig. 10a), Al_2O_3 became discontinuous because of crystallization (Fig. 10b), which showed the same result with in situ experiment in Ref. [26].

4 Discussion

4.1 Composition of the Composites

The oxidation and nitridation processes depended largely on the crystallization of am-Al_2O_3, which could be analyzed from the annealing experiments. In the annealing process, it was found that at 520 °C, no change was revealed in sample AM via strength testing until the annealing time prolonged to 4 h (Fig. 9). Therefore, it can be considered that in the pre-treatment process of samples 400 and 500, am-Al_2O_3 remained its amorphous

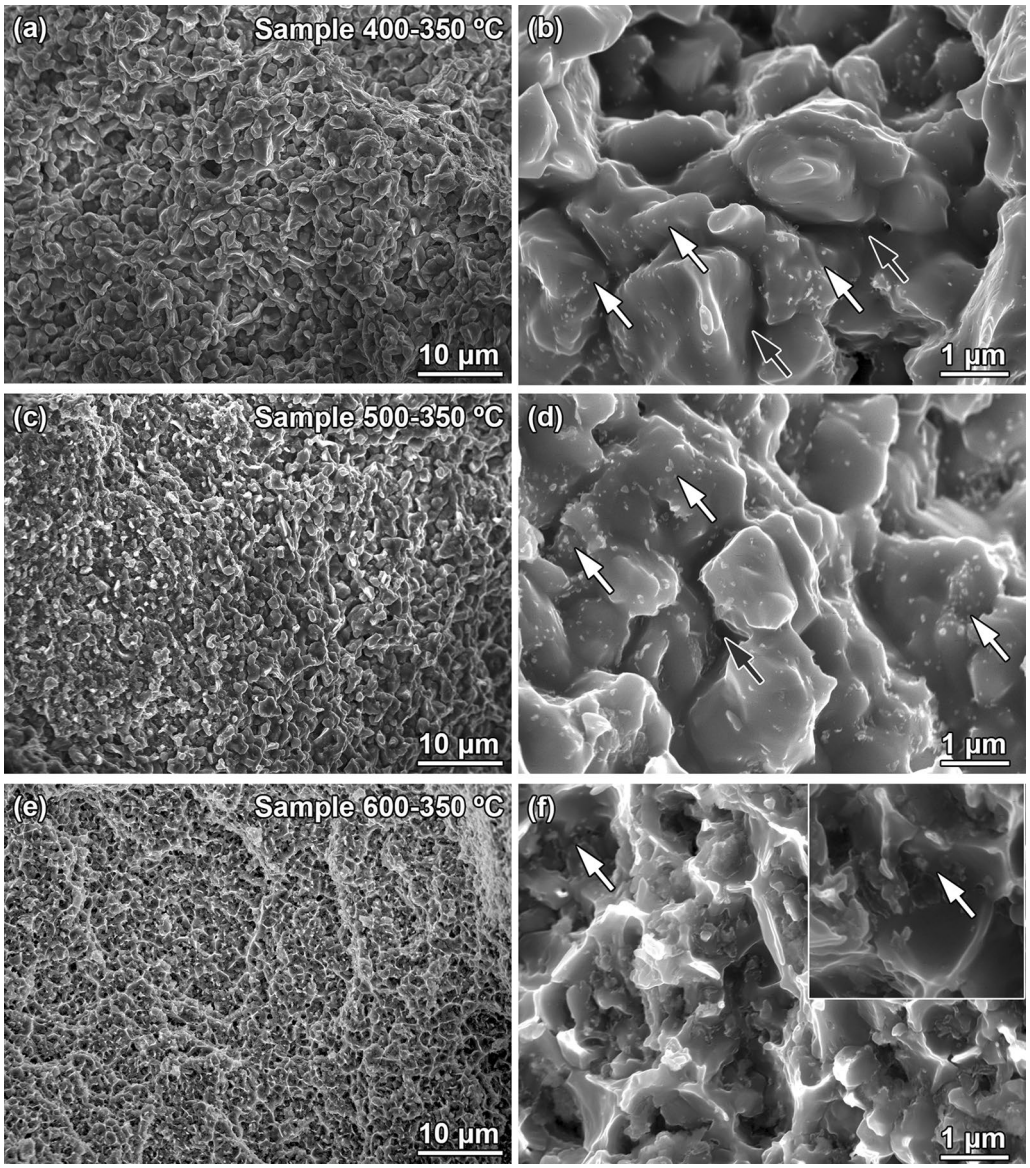

Fig. 8 SEM fractographs of samples 400 **a**, **b**, 500 **c**, **d** and 600 **e**, **f** at 350 °C with different magnifications

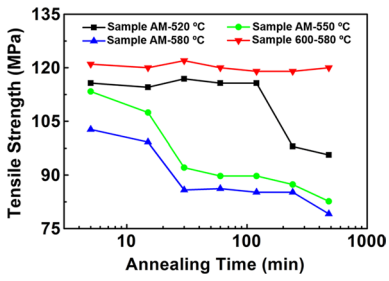

Fig. 9 Variation of tensile strength at 350 °C with annealing time for sample AM annealed at 520 °C, 550 °C and 580 °C, and sample 600 annealed at 580 °C

film morphology and the Al matrix could not be exposed to air. In this case, the oxidation process could only proceed slowly. After pre-treated at 580 °C for 30 min, the strength of sample AM at 350 °C decreased rapidly to 85 MPa (73% of the as-extruded sample). However, when samples were annealed at 550 °C, the same strength loss was realized after over 4 h. Thus, it can be concluded that crystallization of am-Al_2O_3 at 550 °C was still deficient. Therefore, it can be speculated that underlying Al matrix could not be exposed thoroughly and the quantity of introduced particles was still low.

At 600 °C, crystallization of am-Al_2O_3 could be much quicker and more thorough. After the Al matrix was exposed to air, γ-Al_2O_3 would form until the Al powders were fully

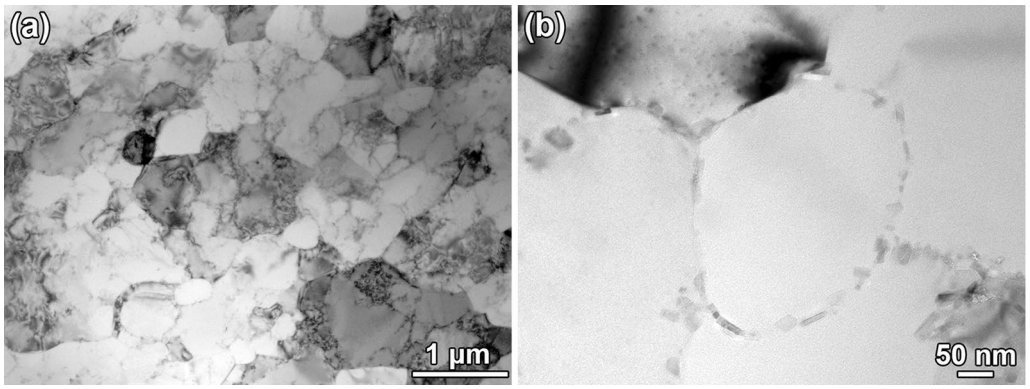

Fig. 10 TEM images showing grain structure **a** and γ-Al_2O_3 **b** in sample AM-annealed at 580 °C for 2 h

covered with nanoparticles. More importantly, N_2 in air could react with Al powders at over 590 °C by the reaction [21, 22]:

$$2Al + N_2 \rightarrow 2AlN. \quad (1)$$

Furthermore, when O_2 was consumed in the cold-compacted bullet and could not be replenished by the incoming gas in time, the oxygen partial pressure in the gas would decrease to a critical value, resulting in the following reaction [22]:

$$2Al_2O_3 + 2N_2 \rightarrow 4AlN + 3O_2. \quad (2)$$

Therefore, a mass of AlN particles were formed and covered fully the Al powders together with γ-Al_2O_3.

4.2 Mechanical Properties of the Composites

At RT, the strength increase came mainly from three mechanisms: (1) fine grain strengthening (Hall–Petch strengthening); (2) direct strengthening of nano-sized particles by load-transfer effect and (3) indirect strengthening of nano-sized particles by dislocation accumulation [15, 27].

With the increase in pre-treatment temperature, more nano-sized particles were introduced on the Al powder surface; therefore, finer grain structure was generated in the extrusion process. Consequently, by considering these three mechanisms mentioned above, the RT strength of the composites increased with increasing the pre-treatment temperature, and when it increased to 600 °C, more drastic oxidation/nitridation process resulted in higher nano-sized particle content; therefore, much higher strength was obtained.

At high temperatures, the GBs were more active in sliding, migration and grain rotation, thereby losing their strengthening effect [15, 18]. Therefore, nano-sized particles located at the GBs could contribute to higher tensile strength [15] and the strength increased with increasing the pre-treatment temperature and particle content. For samples 400, 500 and 550 with relatively fewer nano-sized particles, during the high-temperature tensile process, the GBs could still slide and migrate, and thus, these samples exhibited lower strengths. The composite microstructure evolution largely depended on these nano-sized particles with evolved GBs being pinned by them [13, 28, 29]. During the deformation process of the composites with intergranular nano-sized particles, dynamic recovery would happen at the GBs, and dislocations interacted with the GB Al_2O_3 particles, resulting in localized plastic deformation and void formation [23]. As a result, intergranular fracture happened and γ-Al_2O_3 particles were exposed on the fracture surfaces, as shown in Fig. 8a–d.

For sample 600, the GBs in the as-extruded samples were firmly pinned by (AlN + γ-Al_2O_3) particles, making the GBs extremely stable during the tensile process. Deformation was harder to initiate, resulting in much higher strength. GB sliding, grain rotation and intergranular fracture were severely confined, which can be confirmed by Fig. 8e and f. As only a small number of nano-sized particles exposed on the fracture surface (Fig. 8f), the fracture initiate point was more likely located in the near-GB zones, instead of at the GBs. This could further confirm that strength of the GBs was greatly enhanced.

At high temperatures, dynamic recovery process during tensile deformation could annihilate dislocations, resulting in lack of work hardening. More amount of deformation was accomplished by GB gliding. For samples 400, 500 and 550 with fewer nano-sized particles, high-temperature elongation was higher than that at RT. On the contrary, for samples 600 and AM, the GBs were pinned more firmly, and the elongation became lower at 350 °C. This phenomenon was consistent with other studies [9, 18].

In conclusion, although the strengthening efficiency of (AlN + γ-Al_2O_3) particles was lower than that of lamellar am-Al_2O_3, it was confirmed that the integral strengthening effect could be compensated to even a higher value by introducing more particles via controlling pre-treatment

temperature. More importantly, compared to am-Al_2O_3/Al composites, the newly developed (AlN + γ-Al_2O_3)/Al exhibited extremely enhanced thermal stability. Thus, an effective method to fabricate high-temperature Al was developed in this study.

5 Conclusions

1. High-temperature pre-treatment of the Al powders could introduce nano-sized particles into the Al matrix. The γ-Al_2O_3 concentration increased with the increase in pre-treatment temperature, and when pre-treatment temperature increased to 600 °C, nitridation further happened, resulting in nearly continuous distribution of intergranular (AlN + γ-Al_2O_3) particles in the composite.
2. When the pre-treatment temperature was ≤ 550 °C, the strength of the composites at room temperature and 350 °C could increase with treatment temperature but not reach a value comparable to that for am-Al_2O_3/Al. This was attributed to the softening of grain boundaries (GBs) at high temperatures, resulting in intergranular fracture.
3. Large numbers of intergranular (AlN + γ-Al_2O_3) particles introduced in pre-treatment process at 600 °C could efficiently enhance the GBs and suppress GB sliding and intergranular fracture. Therefore, (AlN + γ-Al_2O_3)/Al exhibited higher strength than am-Al_2O_3/Al at both room temperature and 350 °C.
4. The (AlN + γ-Al_2O_3)/Al did not exhibit the high-temperature strength degradation after annealing treatment at temperatures as high as 580 °C for 8 h, showing obvious superiority compared to am-Al_2O_3/Al that exhibited significant strength decrease when the annealing time exceeded 30 min at 580 °C.

Acknowledgements This work was supported by the National Natural Science Foundation of China (Nos. U1508216 and 51771194), the Youth Innovation Promotion Association CAS (No. 2016179), and the National Key R&D Program of China (No. 2017YFB0703104).

References

[1] T. Sakamoto, S. Kukeya, H. Ohfuji, Mater. Sci. Eng. A **748**, 428 (2019)
[2] L. Zhu, T.S. Liu, T.T. Duan, T.T. Li, F. Qiu, H.Y. Yang, Z.H. Bai, Y.Y. Liu, Q.C. Jiang, Mater. Des. **181**, 107945 (2019)
[3] X.Z. Kai, S.M. Huang, L. Wu, R. Tao, Y.J. Peng, Z.M. Mao, F. Chen, G.R. Li, G. Chen, Y.T. Zhao, J. Mater. Sci. Technol. **35**, 2107 (2019)
[4] Y.H. Gao, C. Yang, J.Y. Zhang, L.F. Cao, G. Liu, J. Sun, E. Ma, Mater. Res. Lett. **7**, 18 (2019)
[5] K. Hu, Q. Xu, X. Ma, Q. Sun, T. Gao, X. Liu, J. Mater. Sci. Technol. **35**, 306 (2019)
[6] H. Junaedi, M.F. Ibrahim, H.R. Ammar, A.M. Samuel, M.S. Soliman, A.A. Almajid, F.H. Samuel, J. Compos. Mater. **50**, 2871 (2016)
[7] J. Qin, Z. Zhang, X.G. Chen, Metall. Mater. Trans. A **47A**, 4694 (2016)
[8] G.J. Li, H.C. Liao, X.J. Suo, Y.Y. Tang, U.S. Dixit, P. Petrov, Mater. Sci. Eng. A **709**, 90 (2018)
[9] C. Poletti, M. Balog, F. Simancik, H.P. Degischer, Acta Mater. **58**, 3781 (2010)
[10] Y.T. Zhou, Y.N. Zan, S.J. Zheng, X.H. Shao, Q.Q. Jin, B. Zhang, X.L. Ma, B.L. Xiao, Q.Z. Wang, Z.Y. Ma, J. Mater. Sci. Technol. **35**, 9 (2019)
[11] W.S. Tian, Q.L. Zhao, Q.Q. Zhang, Q.C. Jiang, Mater. Sci. Eng. A **717**, 105 (2018)
[12] Y.N. Zan, Q. Zhang, Y.T. Zhou, Q.Z. Wang, B.L. Xiao, Z.Y. Ma, J. Nucl. Mater. **526**, 151788 (2019)
[13] L. Wang, F. Qiu, Q.L. Zhao, M. Zha, Q.C. Jiang, Sci. Rep. **7**, 4540 (2017)
[14] A.J. Ardell, Metall. Trans. A **16**, 2131 (1985)
[15] Y.N. Zan, Y.T. Zhou, H. Zhao, Z.Y. Liu, Q.Z. Wang, D. Wang, W.G. Wang, B.L. Xiao, Z.Y. Ma, Compos. Part B **183**, 107674 (2019)
[16] X. Ma, Y.F. Zhao, W.J. Tian, Z. Qian, H.W. Chen, Y.Y. Wu, X.F. Liu, Sci. Rep. **6**, 34919 (2016)
[17] M. Balog, P. Krizik, M. Nosko, Z. Hajovska, M.V.C. Riglos, W. Rajner, D.S. Liu, F. Simancik, Mater. Sci. Eng. A **613**, 82 (2014)
[18] M. Balog, C. Poletti, F. Simancik, M. Walcher, W. Rajner, J. Alloys Compd. **509**, S235 (2011)
[19] Z.Q. Yang, L.L. He, J. Chen, H.T. Cong, H.Q. Ye, J. Mater. Res. **18**, 272 (2003)
[20] L.P.H. Jeurgens, W.G. Sloof, F.D. Tichelaar, E.J. Mittemeijer, Phys. Rev. B **62**, 4707 (2000)
[21] M. Balog, R. Krizik, M. Yan, F. Simancik, G.B. Schaffer, M. Qian, Mater. Sci. Eng. A **588**, 181 (2013)
[22] G.B. Schaffer, B.J. Hall, Metall. Mater. Trans. A **33**, 3279 (2002)
[23] Y.N. Zan, Y.T. Zhou, Z.Y. Liu, Q.Z. Wang, W.G. Wang, D. Wang, B.L. Xiao, Z.Y. Ma, Mater. Sci. Eng. A **773**, 138840 (2019)
[24] T.J. Rupert, D.S. Gianola, Y. Gan, K.J. Hemker, Science **326**, 1686 (2009)
[25] A.T. Lim, D.J. Srolovitz, M. Haataja, Acta Mater. **57**, 5013 (2009)
[26] M. Balog, T. Hu, P. Krizik, M.V. Castro Riglos, B.D. Saller, H. Yang, J.M. Schoenung, E.J. Lavernia, Mater. Sci. Eng. A **648**, 61 (2015)
[27] Y.N. Zan, Y.T. Zhou, Z.Y. Liu, G.N. Ma, D. Wang, Q.Z. Wang, W.G. Wang, B.L. Xiao, Z.Y. Ma, Mater. Des. **166**, 107629 (2019)
[28] W. Kim, S.H. Lee, Compos. Part A **67**, 308 (2014)
[29] S.H. Wang, P.W. Kao, Acta Mater. **46**, 2675 (1998)